1-D Simulation of Ultrafast-Pulsed Laser into Nano-Sized Multilayered Structure (Ni₈₁Fe₁₉/Cu/YIG/GGG) for Memory Device Applications

Muhaiman A. Abdul-Hussain, Haidar J. Mohamad*, Ahmed Al-Haddad

Department of Physics, College of Science, Mustansiriyah University, Baghdad, IRAQ

Abstract

Spintronic offers a solution by exploiting spin instead of electron charge since spin current propagation can occur in principle without dissipation. One of the applications involve within this project for storage media is heat-assisted magnetic recording (HAMR). The objective of this study is to simulate the behavior of thermal gradient to generate a pure spin current using an ultrafast femtosecond (fs) laser in a nano-sized multilayered structure of (Al_2O_3/$Ni_{81}Fe_{19}$ (Py)/Cu/$Y_3Fe_5O_{12}$ (YIG)/$Gd_3Ga_5O_{12}$ (GGG)) at room temperature. A ferromagnetic/spacer/magnetic insulator nano-sized multilayered is the proposed structure for this study. Electron spin, directed by the external applied magnetic field, is transferred via the spacer to the magnetic insulator, leading to the generation of a spin-wave within the last layer. The ultrafast laser generates a spark of spin diffusion to get spin current. The thermal behavior within the trilayer simulated using COMSOL Multiphysics (v 5.5) is presented and supported by the theoretical model. Simulation results showed the effect of thickness and time on the generated spin current. Moreover, the thickness of the permalloy layer plays an essential role in generating a high-temperature gradient within a magnetic insulator to generate a spin current.

Keywords: Spintronics, Spin current; Femtosecond laser; Ferromagnetic materials; COMSOL Multiphysics; HAMR; Nano-sized multilayered structure.

محاكاة بعد واحد لنبضات ليزر فائق السرعة داخل نموذج متعدد الطبقات حجم نانوي (Ni₈₁Fe₁₉/Cu/YIG/GGG) لتطبيقات أجهزة الذاكرة

مهيمن علي عبد الحسين، حيدر جواد محمد*، احمد شكر الحداد

قسم الفيزياء، كلية العلوم، الجامعة المستنصرية، بغداد، العراق

الخلاصة

تقدم تقنية البرم حلاً من خلال استغلال برم الالكترون بدلاً من شحنة الإلكترون لأن انتشار تيار البرم يمكن أن يحدث من حيث المبدأ دون تبديد. أحد التطبيقات التي يتضمنها هذا المشروع لوسائط التخزين هو التسجيل المغناطيسي بمساعدة الحرارة (HAMR). الهدف من هذه الدراسة هو محاكاة سلوك التدرج الحراري لتوليد تيار البرم باستخدام ليزر فيمتوثانية فائق السرعة (fs) في نموذج متعدد الطبقات بحجم النانو (/ Al_2O_3 (GGG) $Gd_3Ga_5O_{12}$ / (YIG) $Y_3Fe_5O_{12}$ / Cu / (Py) $Ni_{81}Fe_{19}$) في درجة حرارة الغرفة. النموذج المقترح لهذه الدراسة هو فيرومغناطيسي / فاصل / عازل مغناطيسي متعدد الطبقات بحجم النانو. ينتقل برم الإلكترون عبر الفاصل إلى العازل المغناطيسي مع برم موجه بواسطة المجال المغناطيسي الخارجي، مما

---

*Email: haidar.mohamad@uomustansiriyah.edu.iq

يؤدي إلى توليد موجة برم داخل الطبقة الأخيرة. يولد الليزر فائق السرعة شرارة لانتشار البرم للحصول على

تيار البرم. يتم وصف السلوك الحراري داخل الطبقة الثلاثية المحاكاة باستخدام COMSOL Multiphysics

(الإصدار 5.5) ودعمه بواسطة النموذج النظري. أظهرت نتائج المحاكاة تأثير السمك للعينة والوقت على تيار

البرم المتولد. علاوة على ذلك ، يلعب سمك طبقة فيرومغناطيسية دورًا أساسيًا في توليد عالي تدرج الحرارة

داخل عازل مغناطيسي لتوليد تيار البرم..

1. Introduction

Pure spin currents that are unassociated to charge transport, can control a new generation of environmentally sustainable and energy-sensitive spintronic (electron spin in electronics) systems. The absorption by a ferromagnetic (FM) layer results angular momentum that occurs during spin currents. This can cause or adjusts the dynamics of magnetization by producing a torque of a spin-transfer [1-3]. Recently, considerable effort has been spent in obtaining spin current, whether by thermal gradients via Seebeck effects [4-8], or the spin current synthesized by the spin hall effect, in which spin-orbit interaction (SOI) is used [9-12]. Moreover, the ultrafast laser generates a spark of spin diffusion to obtain the spin current. This can be result from spin current using an ultrafast fs laser in a multilayer thin film. Frequently, Heat-Assisted Magnetic Recording (HAMR) is considered a technique that requires increasing memory capacities [13]. Bit-Patterned Media (BPM) [14], Shingled Magnetic Recording (SMR) [15] and Microwave-Assisted Magnetic Recording (MAMR) [16] are other recording techniques for improving the density of hard disk storage. The amount of data transferred between the head and the media is much higher in HAMR [17]. Therefore, the high temperature due to the laser within HAMR to transfer data remains a task that needs to be addressed [18].Chen et al.presented a study of the head-disk interface in hard disk drives, which comprises the surface of a disk and a slider surface moving at a different relative velocity [19].

Kiely *et al*. presented a study of the driving forces, mechanisms of the growth, and write-stimulated head contamination growth rates. The combination between an evaporation and condensation model with shear forces proposes that the flow of the lubricant on the head might cause contamination[20]. Sakhalkar and Bogy presented the effect of head, media temperature, and the thickness of lubricant on the lubricant transfer process [21], claiming that initially largely thermally driven was due to the transfer mechanism. According to a previous study, Mohamad et al. succeeded in experimentally generating spin current by ultrafast laser in multilayer thin films, but they did not consider the effect of ferromagnetic layer thickness on the spin current generation, which can be explored in detail by studying the effect of the layer thickness[22].

In the present study, a thermal behavior, induced by ultrafast fs laser within the nano-sized trilayer $Ni_{81}Fe_{19}$ (Py)/Cu/$Y_3Fe_5O_{12}$ (YIG) using COMSOL Multiphysics (v 5.5)was simulated, where a one-dimensional model was designed. The ferromagnetic over-layer is partially demagnetized by the fs laser pulse, resulting in a high thermal gradient within the trilayer structure sample. Electron spin is passed to the magnetic insulator through a spacer. Thereby, spin current, which plays an important role in spintronic devices and their applications, was obtained. The challenge is to simulate the ultrafast pulsed laser and study the temperature gradient within the sample as a function of time and sample thickness. Therefore, both ferromagnetic and magnetic insulator are important in this case. Ultra fast pulsed laser generates heat along all layers with different percentage due to the layer heat conductivity.

2. Theoretical Consideration

Within the time scale of the femtosecond, pulses of ultrafast laser energy can penetrat into the sample layers. The temperature increases rapidly within the sample, therefore it is easy to be explained by the one-dimensional heat diffusion equation [23]. Many important studies have

focused on the heat diffusion equation within a metal [24] to describe the electron, lattice, and spin interaction [25]. The description of this interaction is written as [26]:

$$\frac{1}{D}\frac{\partial T}{\partial t} = \frac{\partial^2 T}{\partial z^2} + \frac{g(z,t)}{k} \tag{1}$$

Where z is a layer thickness, T is the temperature, t is time, and $g(z, t)$ is the absorbed power density in the sample. Thermal diffusivity D could be represented by ($D = k /\rho\, C_p$), where k, ρ, C_p are the thermal conductivity, the material density, and the heat capacity per unit mass, respectively. All these parametres are well known and were collected from different litretures. Spin current describes the flow of spin angular momentum within materials. The waveform shape of a spin current equals in energy term flipping the spin magnetization from up to down. This saves energy on the microscopic scale and leads to the spintronic devices. The structure of the spintronic device is vital; therefore, the suggested structure is considered to generate   spin current within the nano-sized YIG layer. Using an ultrafast laser directed to the sample structure, the temperature gradient was solved. The sample structure considered is a trilayer   of ferromagnetic/spacer/magnetic insulators. Inside the trilayer sample, the transient temperature distribution has cylindrical symmetry. Since the stack thickness is of a lower value than the diameter of the laser spot, lateral heat diffusion at the sample's surface can be overlooked. The absorbed power density (heat source) in the heat diffusion equation and the temperature in each layer in the stack were determined using the distribution of the electric field in the active layer(s). By considering multiple reflection and propagation, the model specified the transmission/reflection coefficients at the film interfaces [27]. Only the (lossy) permalloy and/or copper layers are thought to absorb light; the other layers in the stack have either comprehensive or negligible value of the extinction coefficients (imaginary part of the refractive index - k_m). Consequently, only a two-layer absorption model as shown in Figure 1 was used here, with the outer layers considered to be semi-infinite in extent.

The Poynting vector links a complex wave's time-averaged power per unit area (W/m^2) to electric and magnetic fields by the relation:

$$\langle \boldsymbol{S}_m \rangle = \frac{1}{2}\operatorname{Re}\{\boldsymbol{E}_m \times \boldsymbol{H}_m^*\} \tag{2}$$

The normalized power density can be written as[28, 29] :

$$\operatorname{Re}\left\{ -\nabla \cdot \frac{\langle S_m \rangle}{\langle S_i \rangle} \right\} = 2k_0 \frac{n_m k_m}{n_i} \frac{|E_m|^2}{I_i^2} \tag{3}$$

where $\langle S_i \rangle$ is the time-averaged power density of the incident electric field, k_0 is the wave number at the laser wavelength ($k_0 = 2\pi/\lambda$), n_m and n_i are the refractive indices of the transmitted and incident media, respectively, E_m is the transmitted electric field in layer m, and I$_i$ is the incident electric field magnitude that takes the form $I_i^2 = \tau_{12}^2 E_1^2$ for the first layer, where $\tau_{12} = 2n_1/(n_1 + n_2)$, n_1 and n_2 being the refractive indices of the incident and transmitted media. For air/Al$_2$O$_3$ interface, n_1 and n_2 represent the refractive index of air and Al$_2$O$_3$ layer, respectively. Figure 1 presents the optical system that was used to simulate laser beam that has high penetration depth.
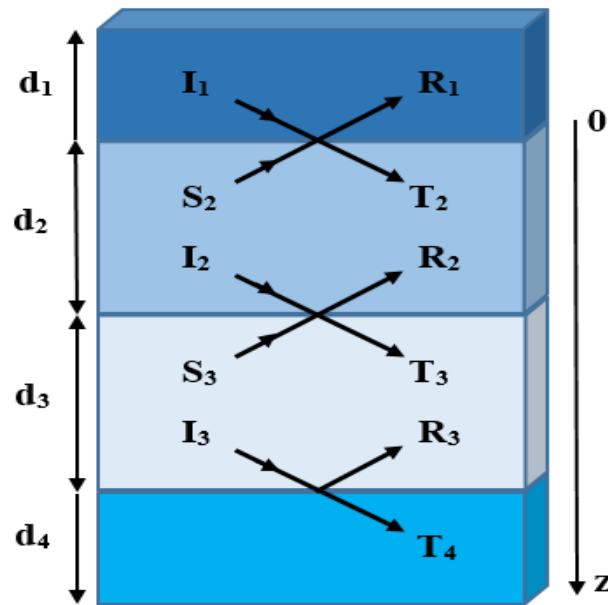
Figure 1-The transmission/reflection model within the multilayer concept. I, R and T are the incidents, reflected, and transmitted field amplitudes respectively, while S is the amplitude of the field reflected from the next interface, d is the layer thickness [27].

3. Experimental Consideration

The model is described in theoretical consideration and was achieved using simulation software COMSOL Multiphysics version 5.5. A one-dimensional model was build using a time-based study in heat transfer in solids (ht) interface as shown in Figure 2. The model was based on the measurement of a multilayer thin metallic film (Al_2O_3/Cu/$Ni_{81}Fe_{19}$/YIG/GGG) heated by an ultrafast laser, as shown in Figure 3. The sample was not damaged by the laser pulses due to its properties. The theoretical concepts considered the 3D tempreture model which determine the lattice, electron, and spin relationship. The data of materials parameters was taken from previous works [30-35]. A summary of these parameters with descriptions and corresponding references are presented in Table 1. The geometry of the sample was made as shown in Figure 4. The laser pulse plays an essential role in this work, as it represents the source of heat falling on the sample, which has a Gaussian shape and spot diameter of 120 μm. The FWHM laser pulse width (t) is assumed to be 74 fs, while the laser repetition rate (f) is 100 kHz. Therefore, the peak power (P) in mW takes the following form[36]:

$$P = \frac{\text{power }(mW)}{f \times t} = \text{ power }(mW) \times 1.3514 \times 10^8 \tag{4}$$

Thermal-Boundary Resistance (TBR) interface conditions were used in the numerical simulations in COMSOL software to account for the imperfect interaction between the various layers in the stack of multi-nano-size composite layer. The TBR values related to the interfaces between each layer in the structure are not well understood and are dependent on the structure of the interface formation[37]. An assumed value of $1/R_{th}$ was (2×10^8 W/m^2/K) for the Al_2O_3/$Ni_{81}Fe_{19}$ and Cu /YIG interfaces [38, 39], whereas the values of (1×10^9 and 2.04×10^8 W/m^2/K) were gathered for $Ni_{81}Fe_{19}$ /Cu and YIG/GGG [39], respectively. Figure 2 shows the front layout of the Comsol software with the designed code for the presented sample. Figure 3 (a) presents the studied sample in 3D design with the input laser beam. Figure 3 (b) shows the sketch of the spin current (J) and the concept of the spin transfer [22]. While, Figure 4 shows the final 1D designed code and the line on the top of the figure was drawn to clarify   the sample structure only.
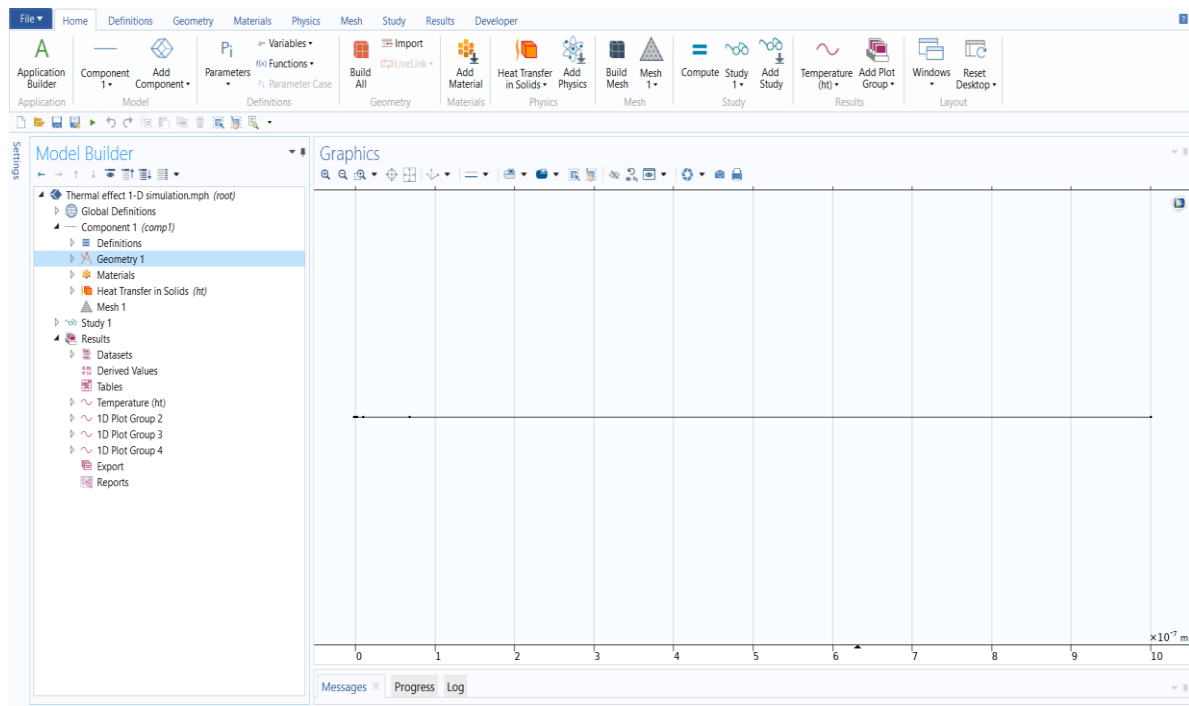
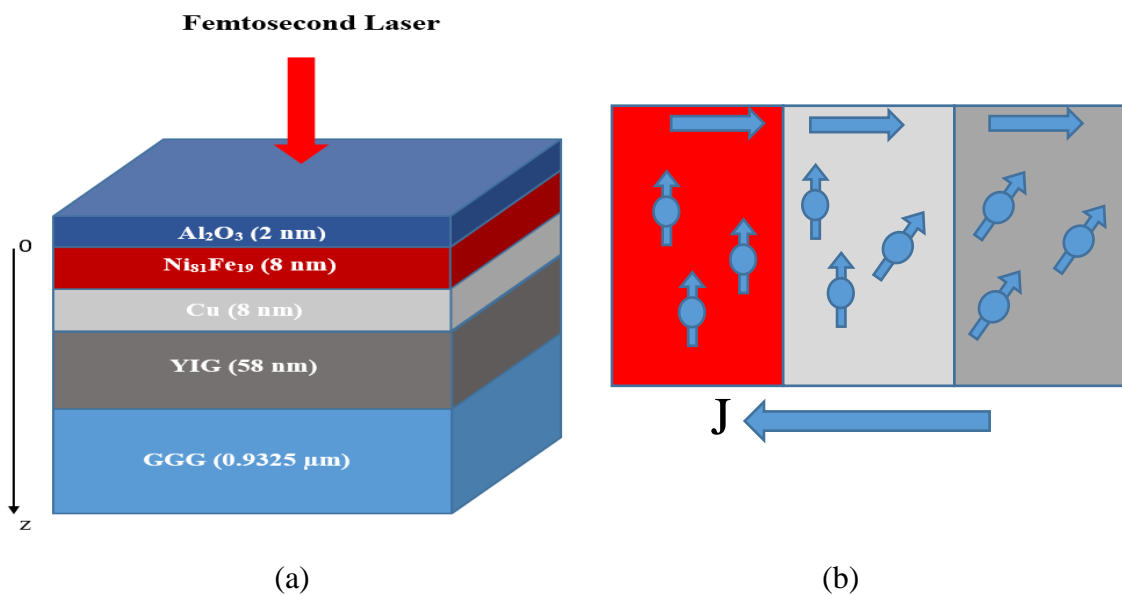**Figure 2**-One-dimensional model interface in COMSOL Multiphysics.

Femtosecond Laser

(a)   (b)

Figure 3-(a) Trilayer sample stack in which the absorption of the optical power is expected for the Ni81Fe19 and Cu layers only, and (b) the concept of Spin Transfer Torque.
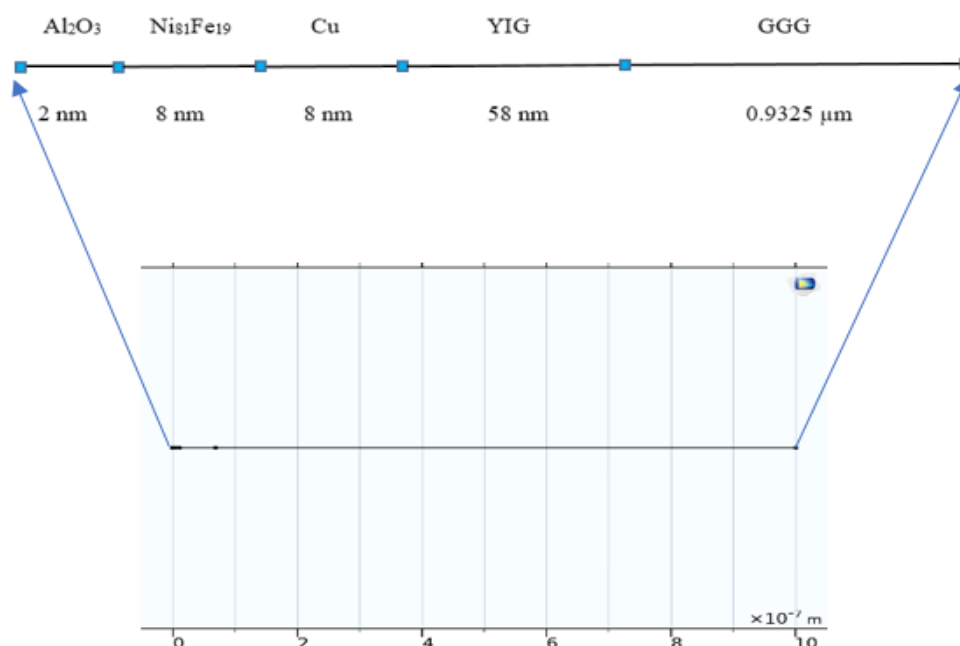
Figure 4-The COMSOL Multiphysics geometry of the sample in a one-dimensional model, with a schematic showing the thickness of each layer.

Table 1-The assumed values of the thermal and optical calculations at a temperature of 300 [the values of parameters were dependent on standard data, except where indicated otherwise].

Parameter Unit	Al_2O_3	Py	Cu	YIG	GGG
Density kg/m^3	3890	8700	8930	5170	7080
Thermal conductivity W/m/K	1–4.5 [30]	46.4 [31]	150 [32]	6.63 [33]	7.94 [33]
Heat capacity J/kg/K [28]	880	430	385	578	400
Refractive index n (800 nm)	1.759	2.2 + j3.6 [34]	0.24991 + j5.0337	$2.19 + j2.48 \times 10^{-6}$ [35]	1.95

4. Results and Discussion

Simulation results describe the effect of time and thickness in generating spin current induced by optical pumping within a trilayer (Py/Cu/YIG). The temperature profile within the sample at different time delays is shown in Figure 5 with the inclusion of TBR. The time dependence of the change in temperature at designated depths in the sample is revealed in Figure 6 with the inclusion of TBR. The temperature gradient at different positions within the YIG layer is plotted in Figure 7. Change in temperature as a function of the depth of Py within the YIG sample at time 0.05 ns is shown in Figure 8.
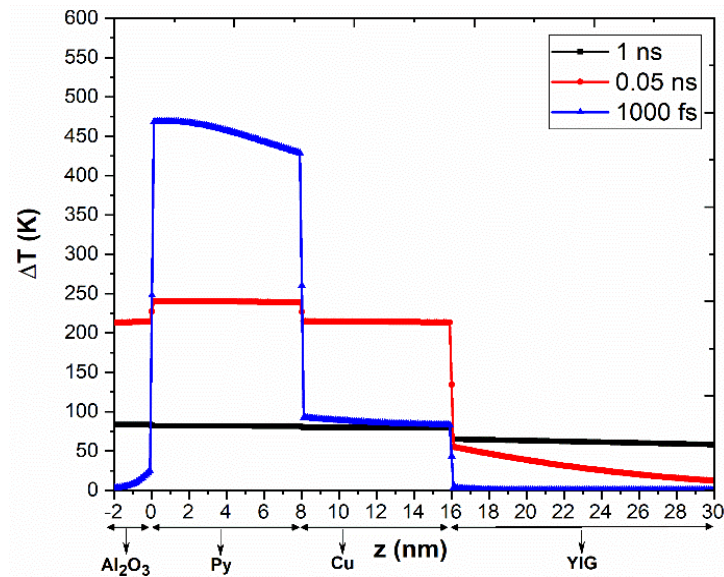
Figure 5-Temperature as a function of trilayer structure depth at each delay of the time, the calculation includes TBR.

Thermal modeling in Figure 5 illustrates the relationship between temperature variation with depth that occurs in the trilayer sample as a result of excitation by fs laser pulse at selected time intervals. A significant rise in the temperature of the permalloy layer was observed, also an increase in the energy absorption in the copper film was noted , which leads to a thermal gradient inside the sample (YIG) at a time of 1 and 0.05 ns, indicating the generation of spin current.
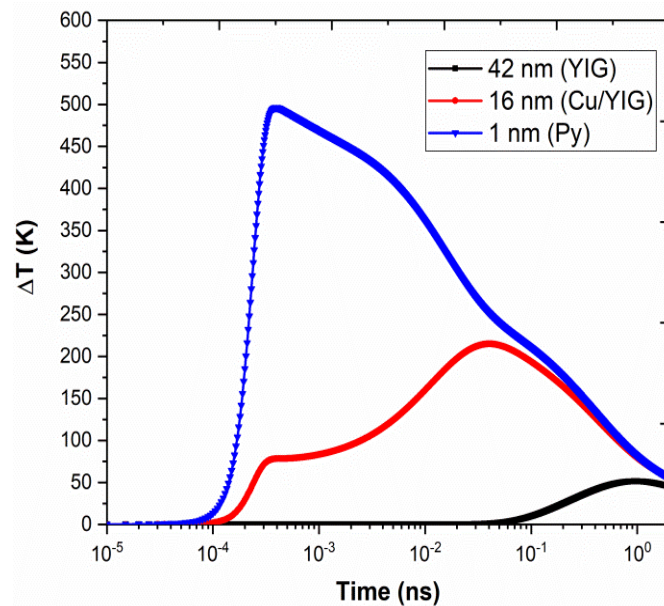

Figure 6-Relation between temperature change and the time at selected depths in the trilayer structure, the calculation includes TBR.

Figure 6 describes the time dependence of the change in temperature at selected depths in the structure with the addition of TBR. Since the YIG is translucent, thermal conduction occurs by the first two layers allowing the temperature inside the YIG layer to increase on a time scale of about 1 ns. In the Cu/YIG interface, a marked rise in temperature over a time scale of 0.05 ns was observed, indicating the importance of including TBR in the calculations.
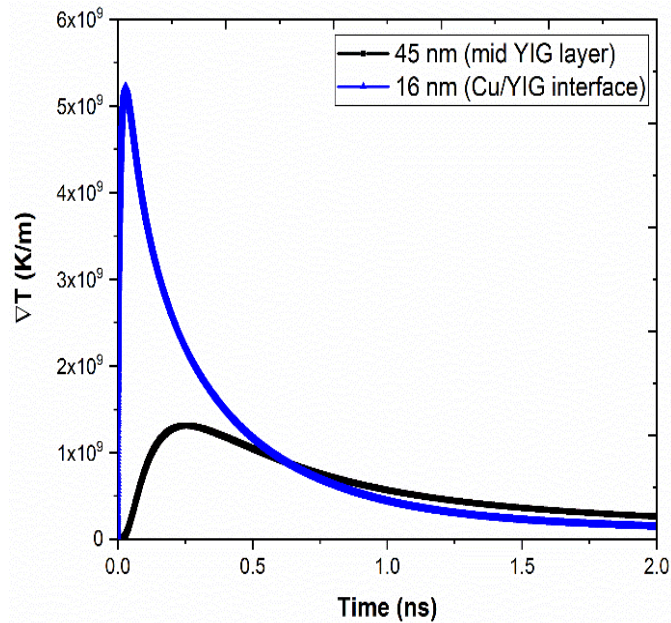
Figure 7-Temperature gradient as a function of time in the trilayer structure. The value [1/Rth = 2×108 W/m²/K] is assumed for Cu/YIG interface.

The temperature gradient is shown in Figure 7, which is highly influenced by the sample's position z relative to the surface. The presence of a large thermal gradient at the Cu/YIG interface highlights the importance of using TBR in the calculations.
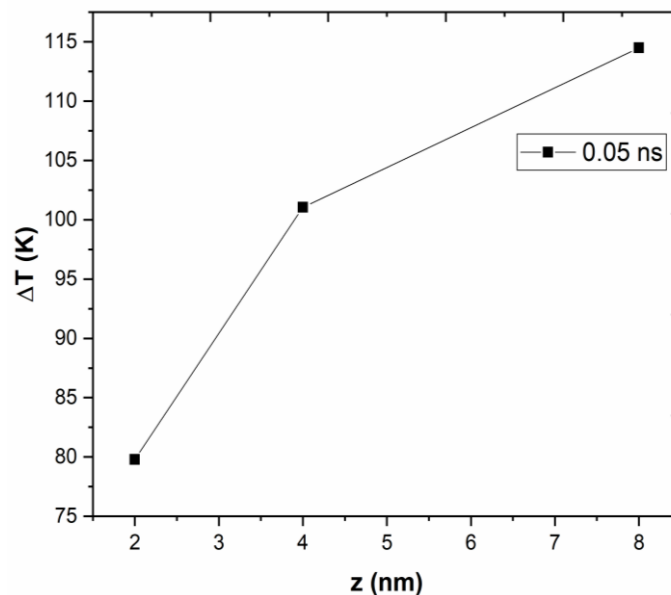

Figure 8-Temperature and depth relation of Py within the YIG layer at time 0.05 ns, the calculation includes TBR.

The temperature change in the YIG layer at different permalloy layer thicknesses is shown in Figure 8. The change in the thickness of the Py leads to an increase in the temperature difference in the YIG layer. This can save energy and use small power with the applied laser. The maximum temperature was observed at 8 nm thickness and 0.05 ns time.

5. Conclusion
The HAMR is considered a challenging task to explore due to the microscopic details that need to be addressed. This study presented a simulation of spin current in a one-dimensional

model. The spin current was generated by the temperature gradient within the magnetic insulator (YIG). The obtained simulation results described the effect of thickness and time on the generation of spin current induced by optical pumping within a trilayer (Py/Cu/YIG). The Cu/YIG interface was noticed to be very important in the spin current generation, indicating the importance of including TBR values in calculations. Furthermore, it was shown that the thickness of the permalloy layer is essential in generating a high-temperature gradient within the magnetic insulator in order to generate spin current. This leads to reducing the laser power used to generate the temperature gradient within the sample and so energy is saved.

References
[1] G.-M. Choi, B.-C. Min, K.-J. Lee, and D. G. J. N. c. Cahill, "Spin current generated by thermally driven ultrafast demagnetization," vol. 5, no. 1, pp. 1-8, 2014.
[2] G. Manfredi, J. Hurst, and P.-A. Hervieux, "Ultrafast spin current generation in ferromagnetic thin films," in Spintronics XI, vol. 10732: International Society for Optics and Photonics, pp. 107322V, 2018.
[3] S. Huang, D. Qu, T. Chuang, C. Chiang, W. Lin, and C. J. A. P. L. Chien, "Pure spin current phenomena," vol. 117, no. 19, p. 190501, 2020.
[4] G. Da Silva, L. Vilela-Leão, S. Rezende, and A. J. J. o. A. P. Azevedo, "Spin current injection by spin Seebeck and spin pumping effects in yttrium iron garnet/Pt structures," vol. 111, no. 7, p. 07C513, 2012.
[5] S. D. Brechet, F. A. Vetro, E. Papa, S. E. Barnes, and J.-P. J. P. r. l. Ansermet, "Evidence for a magnetic seebeck effect," vol. 111, no. 8, p. 087205, 2013.
[6] P. Li et al., "Generation of pure spin currents via spin Seebeck effect in self-biased hexagonal ferrite thin films," vol. 105, no. 24, p. 242412, 2014.
[7] F.-J. Chang, J. G. Lin, and S.-Y. J. P. R. M. Huang, "Robust spin current generated by the spin Seebeck effect," vol. 1, no. 3, p. 031401, 2017.
[8] Y. Zhou and X. J. J. o. P. C. M. Zheng, "Generating pure spin current with spin-dependent Seebeck effect in ferromagnetic zigzag graphene nanoribbons," vol. 31, no. 31, p. 315301, 2019.
[9] S. Valenzuela and M. J. J. o. a. p. Tinkham, "Electrical detection of spin currents: The spin-current induced Hall effect," vol. 101, no. 9, p. 09B103, 2007.
[10] L. Liu, C.-F. Pai, Y. Li, H. Tseng, D. Ralph, and R. J. S. Buhrman, "Spin-torque switching with the giant spin Hall effect of tantalum," vol. 336, no. 6081, pp. 555-558, 2012.
[11] L. Zhu, D. C. Ralph, and R. A. J. P. R. A. Buhrman, "Highly efficient spin-current generation by the spin hall effect in Au 1− x Pt x," vol. 10, no. 3, p. 031001, 2018.
[12] A. Kumar, R. Bansal, S. Chaudhary, and P. K. J. P. R. B. Muduli, "Large spin current generation by the spin Hall effect in mixed crystalline phase Ta thin films," vol. 98, no. 10, p. 104403, 2018.
[13] M. H. Kryder et al., "Heat assisted magnetic recording," vol. 96, no. 11, pp. 1810-1835, 2008.
[14] H. Richter et al., "Recording potential of bit-patterned media," *Appl. Phys. Lett.* vol. 88, no. 22, p. 222512, 2006.
[15] G. Gibson and G. J. C. M. P. D. L. Ganger, CMU-PDL-11-107, "Principles of operation for shingled disk devices," 2011.
[16] S. Okamoto, N. Kikuchi, M. Furuta, O. Kitakami, and T. J. J. o. P. D. A. P. Shimatsu, "Microwave assisted magnetic recording technologies and related physics," vol. 48, no. 35, p. 353001, 2015.
[17] G. Ju et al., "High Density Heat-Assisted Magnetic Recording Media and Advanced Characterization—Progress and Challenges," *IEEE Transactions on Magnetics*, vol. 51, no. 11, pp. 1-9, 2015, doi: 10.1109/TMAG.2015.2439690.
[18] S. Xiong, N. Wang, R. Smith, D. Li, E. Schreck, and Q. Dai, "Material Transfer Inside Head Disk Interface for Heat Assisted Magnetic Recording," *Tribology Letters*, vol. 65, no. 2, p. 74, 2017/04/29 2017, doi: 10.1007/s11249-017-0860-6.

[19] Y.-K. Chen, J.-P. Peng, and D. B. Bogy, "Surface evolution of perfluoropolyether film at high speed quasi-contact conditions," *Applied Physics Letters*, vol. 108, no. 22, p. 221602, 2016.

[20] J. D. Kiely et al., "Write-induced head contamination in heat-assisted magnetic recording," *IEEE Transactions on Magnetics*, vol. 53, no. 2, pp. 1-7, 2016.

[21] S. V. Sakhalkar and D. B. Bogy, "A model for lubricant transfer from media to head during heat-assisted magnetic recording (HAMR) writing," *Tribology Letters*, vol. 65, no. 4, p. 166, 2017.

[22] H. Mohamad et al., "Thermally induced magnetization dynamics of optically excited YIG/Cu/Ni 81 Fe 19 trilayers," *Phys. Rev. B*, vol. 96, no. 13, p. 134431, 2017.

[23] M. Makhtoumi, "Numerical solutions of heat diffusion equation over one dimensional rod region," *International Journal of Science and Advanced Technology*, vol. 7, no 3, p.10, 2017

[24] D. Mahardika and F. Haryani, "Numerical analysis of one dimensional heat transfer on varying metal," in *Journal of Physics*: Conference Series, 2020, vol. 1511, no. 1: IOP Publishing, p. 012049.

[25] K. R. O'Neal et al., "Spin–lattice and electron–phonon coupling in 3 d/5 d hybrid Sr 3 NiIrO 6," vol. 4, no. 1, pp. 1-6, 2019.

[26] M. J. J. M. O. A. A. Hancock, "The 1-D heat equation," vol. 31, 2006.

[27] A. J. J. Crook, "The reflection and transmission of light by any system of parallel isotropic films," vol. 38, no. 11, pp. 954-964, 1948.

[28] A. Goswami and P. Sen, "Chapter 4 - Energy Harvesting Using Droplet," in Nanomaterials for Green Energy, B. A. Bhanvase, V. B. Pawade, S. J. Dhoble, S. H. Sonawane, and M. Ashokkumar Eds.: Elsevier, 2018, pp. 113-143.

[29] A. Z. Khalaf and B. H. Alyasery, "Laser Distance Sensors Evaluation for Geomatics Researches," Iraqi Journal of Science, pp. 1831-1841, 2020, doi: 10.24996/ijs.2020.61.7.32.

[30] B. Su-Yuan, T. Zhen-An, H. Zheng-Xing, Y. Jun, and W. J. C. P. L. Jia-Qi, "Thermal conductivity measurement of submicron-thick aluminium oxide thin films by a transient thermo-reflectance technique," vol. 25, no. 2, p. 593, 2008.

[31] A. Avery, S. Mason, D. Bassett, D. Wesenberg, and B. J. P. R. B. Zink, "Thermal and electrical conductivity of approximately 100-nm permalloy, Ni, Co, Al, and Cu films and examination of the Wiedemann-Franz Law," vol. 92, no. 21, p. 214410, 2015.

[32] W. Liu, Y. Yang, and M. Asheghi, "Thermal and electrical characterization and modeling of thin copper layers," in Thermal and Thermomechanical Proceedings 10th Intersociety Conference on Phenomena in Electronics Systems, 2006. ITHERM 2006.: IEEE, pp. 1171-1176, 2006.

[33] A. M. J. P. Hofmeister and C. o. Minerals, "Thermal diffusivity of garnets at high temperature," vol. 33, no. 1, pp. 45-62, 2006.

[34] G. Neuber et al., "Temperature-dependent spectral generalized magneto-optical ellipsometry," vol. 83, no. 22, pp. 4509-4511, 2003.

[35] T. Goto, M. C. Onbaşlı, and C. J. O. e. Ross, "Magneto-optical properties of cerium substituted yttrium iron garnet films with reduced thermal budget for monolithic photonic integrated circuits," vol. 20, no. 27, pp. 28507-28517, 2012.

[36] R. K. Jamal and R. K. Rustum, "Studying the Effect of Laser Pump Pulse Energy and Delay Time on Conversion Efficiency of KTP," *Iraqi Journal of Science*, pp. 351-357, 2020, doi: 10.24996/ijs.2020.61.2.13.

[37] A. Al-Haddad, Z. Wang, M. Zhou, S. Tarish, R. Vellacheri, and Y. Lei, "Constructing Well-Ordered CdTe/TiO2 Core/Shell Nanowire Arrays for Solar Energy Conversion," Small, vol. 12, no. 40, pp. 5538-5542, 2016, doi: 10.1002/smll.201601412.

[38] B. C. Gundrum, D. G. Cahill, and R. S. J. P. R. B. Averback, "Thermal conductance of metal-metal interfaces," vol. 72, no. 24, p. 245426, 2005.

[39] M. Schreier et al., "Magnon, phonon, and electron temperature profiles and the spin Seebeck effect in magnetic insulator/normal metal hybrid structures," vol. 88, no. 9, p. 094410, 2013.